Project funded by the European Commission under the 6th (EC) RTD Framework Programme (2002- 2006) within the framework of the specific research and technological development programme “Integrating and strengthening the European Research Area”

Project UpWind.TTC

Contract No.:
019945 (SES6)

“Integrated Wind Turbine Design”

Model of progressive partial/complete matrix-fiber debonding

AUTHOR:	Dr Volodymyr Kushch
AFFILIATION:	Institute for Superhard Materials NAS of Ukraine
ADDRESS:	2 Avtozavodskaya Str., 04074 Kyiv Ukraine
TEL.:	+38 044 432 9544
EMAIL:	vkushch@bigmir.net
FURTHER AUTHORS:	Sergiy V. Shmegera, Yaroslav O. Podoba, Dr Leon Mishnaevsky Jr
REVIEWER:	Project members
APPROVER:	

Document Information

DOCUMENT TYPE	Deliverable
DOCUMENT NAME:	Model of progressive partial/complete matrix-fiber debonding
REVISION:	
REV.DATE:	
CLASSIFICATION:	R1: Restricted to project members
STATUS:	

Abstract: The model of progressive interface debonding in fiber reinforced composite has been developed based on the cohesive-zone approach. The comparison has been made and the relationship is shown with the standard LFM model. An interface crack nucleation, onset and growth has been studied in detail for a single fiber at first and the effect of CZM parameters on debonding is evaluated numerically. Then, the effect on debonding progress of local stress redistribution due to interaction between the fibers was studied in the framework of two-inclusion model. The full-scale simulation of progressive debonding in FRC using the many-inclusion FCM and RUC models of composite has been performed. It has been shown that the developed model provides reliable prediction of the progressive debonding phenomenon including the interface crack cluster formation, overall stiffness reduction and induced anisotropy of the effective elastic moduli of composite.

Contents

1. Cohesive-zone model of matrix-fiber interface 4

2. Single inclusion problem: interface crack onset and growth 5

2.1 Parametric study and comparison with LFM model 5
2.2 Comparison with experiment 8

3. Two-fiber model: debonding affected by interaction 10

4. FCM and RUC models of progressive debonding: interface crack cluster formation and stiffness reduction 12

5. Conclusions 18

References 18

STATUS, CONFIDENTIALITY AND ACCESSIBILITY										
Status				**Confidentiality**				**Accessibility**		
S0	Approved/Released			**R0**	General public			Private web site		
S1	Reviewed			**R1**	Restricted to project members	**R1**		Public web site		
S2	Pending for review			**R2**	Restricted to European. Commission			Paper copy		
S3	Draft for commends			**R3**	Restricted to WP members + PL					
S4	Under preparation			**R4**	Restricted to Task members +WPL+PL					

PL: *Project leader* **WPL:** *Work package leader* **TL:** *Task leader*

1. Cohesive-zone model of matrix-fiber interface

Non-linearity of the crack propagation (including interface debonding) problem stems from two main sources. First, the same geometry of problem (including crack length, crack tip position, etc.) *varies* during the loading time and thus the problem cannot be regarded as linear. Second, the physical non-linearity stems from the fact that the material/interface (no matter how strong it is) has a *finite* strength and thus stress is finite in any vicinity of a crack tip, in contrast to LMF concept. The only way to get a finite energy release rate (ERR) necessary for crack to propagating is to assume a *finite* length "process zone" of damaged (but not fully separated interface edges) as well.

The obvious fact is that the non-linear problem *in principle* cannot be solved by means of linear fracture mechanics: in the lucky case, we can approach the solution (within a certain accuracy) by a series of LFM problems. The commonly used in literature criteria of interface crack onset and propagation are: (a) stress (*crack nucleation*) criterion: $F(\sigma_r, \tau_{r\theta}) \geq \sigma_c$ (σ_c is an interface strength); (b) energy release rate (*crack propagation*) criterion: $\delta G \geq G_c$ (G_c is a fracture toughness); (c) Linear Fracture Mechanics criteria: stress intensity factor (SIF), crack opening displacement (COD), etc. However, their applicability is confined, as a rule, to the classical Griffith criterion: given a fixed crack and load, to decide whether or not it will propagate? Moreover, the well-known paradox of LFM says that an interface crack onset cannot be correctly predicted by either(!) of these criteria, taken individually (e.g., Leguillon, 2002; Cornett et al, 2006; Taylor, Taylor, 2008). The attempts to resolve this paradox by tailoring the coupled stress and energy criterions (e.g., Mantič, 2009) do not - and cannot! - solve non-linear problem in the framework of linear theory. At the same time, the above mentioned paradox resolves in a simple and physically substantiated way by assuming the behavior non-linear of material (or interface) in a vicinity of the crack tip.

The above reasons renewed interest in the concepts of cohesive-zone models to characterize failure (e.g., Needleman, 1987; Ungsuwarungsri and Knauss, 1987; Tvergaard and Hutchinson, 1992; Xu and Needleman, 1994; Li et al., 2005). These models are refinements of concepts first discussed by Dugdale (1960) and Barenblatt (1962). At their core is the introduction of a second fracture parameter in addition to the toughness, G_c. This second parameter is a characteristic strength σ_c, that relates the toughness to the critical crack-tip opening required for crack advance. The characteristic strength can be thought of as a measure of the maximum strength or, in a more general sense, as a measure of the average strength of the interface. The two fracture parameters of characteristic strength and toughness lead to a length scale for fracture given by EG_c/σ_c^2, where E is the elastic modulus of material. A comparison of this length scale to the characteristic dimensions of the geometry indicates whether the assumptions of linear-elastic fracture mechanics are met. If all characteristic geometrical lengths are significantly bigger than the fracture length scale or, the same, dimensionless number (K-criterion) $G^* = E^*G_c/\sigma_c^2R << 1$, then G_c alone can be used for failure analysis. Otherwise, a cohesive-zone model using both the toughness and characteristic strength must be used to analyze fracture. Not only does the cohesive-zone approach eliminate the length-scale restrictions imposed by conventional fracture-mechanics, but situations in which conventional fracture mechanics is appropriate are easily solved as special cases of the more general cohesive-zone framework. Moreover, the nature of the implementation of cohesive-zones into numerical analysis (e.g., Xu and Needleman, 1994; Alfano and Crisfield, 2001) results in essentially automatic prediction of fracture, providing a smooth transition between different failure regimes.

In what follows, we use the bi-linear cohesive zone model (CZM) suggested by Alfano and Crisfield (2001). The suggested by this model normal stress - normal opening relationship is shown in Fig. 1. It comprises the linearly elastic segment (OA) with contact stiffness Kn and the linear stiffness degradation segment (AC). The max contact stress σ_{max} (= cohesive strength σ_c) reaches in the point A whereas the OA slope depends on the fracture (brittle or viscous) mode.

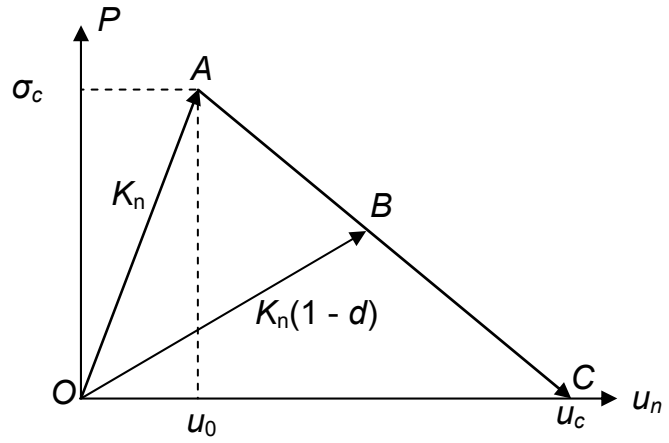

Fig. 1. Bi-linear model of cohesive zone (normal traction)

Crack formation starts in the point A and ends in the point C, where the traction at the newly created crack surface vanishes completely. From A to C the damage parameter d grows linearly, hence unloading and subsequent re-loading goes along the line OB defined by the reduced contact stiffness $K_n(1 - d)$. The triangle OAC area is the nothing else but the crack opening work, or so-called critical fracture energy G_c. Thus, this criterion combines the fracture stress and energy conditions.

It worth to mention as well that this model accounts for the scale factor in a natural way. In Fig. 1 the x-axis shows displacement (contact opening). It means that despite the equal tress state around the congruent (geometrically similar) inclusions, an absolute displacement value is proportional to the inclusion size. Hence, for small inclusions the critical values u_0 and u_{max} are expected at much higher load than for large ones. Other words, "weakening" effect of big inclusion is more pronouncing; in particular, the model predicts existence of critical inclusion size below which interface crack nucleation for a given interface fracture toughness is impossible. This feature agrees well with experimental observations (e.g., Leguillon and Piat, 2008) which can be regarded as an additional argument in favor of the chosen approach.

2. Single inclusion problem: interface crack onset and growth

2.1. Parametric study and comparison with LFM model

We start our analysis with the simplest model being a single fiber embedded in an infinte matrix. However, to the best knowledge of authors, there exists a very few publications (e.g., Tan et al, 2006) where even this type model was studied in the case of adhesive matrix-to-fiber bonding. To minimize a number of the problem parameters, we put the fiber radius R = 1. We consider stress field around the fiber caused by far uniaxial tension; to be specific, we assume it acting in y-axis direction. Following Toya (1974), we put the elastic moduli equal to ν_m = 0.35, μ_m =1 for the matrix material and ν_f = 0.22, μ_f = 44.2/2.39 for the fiber. Also, we put the interface characteristic strength σ_c =1. In order to get the results comparable with those predicted by LFM, we have to meet the condition $E^*G_c/\sigma_c^2\ R << 1$ where $E^* = 1/(1/E_m + 1/E_f)$. This condition implies $G_c << 1$ for σ_{far} = 1; in our first numerical study, we put G_c = 0.004 for both the normal and tangential mode.

The stress field evolution and crack onset is clearly seen from the Figs 2a-2d, where the isolines of max tensile stress σ_1 field are shown corresponding to σ_{far} increasing from 0.80 to 1.0. In fact, for σ_{far} = 0.80, due to stress concentration, the normal interface stress approached σ_c where the interface damage starts to develop. It is seen that stress at the poles is already below the peak value. Soon after that, at σ_{far} = 0.85 (Fig. 2b) we already see distinctive interface crack with traction-free edges. Subsequent load increase lead to steady crack growth: as seen from Fig. 2d, when the crack semi-angle exceeds 60, its propagation becomes more involved and affected by the crack opening/closure.

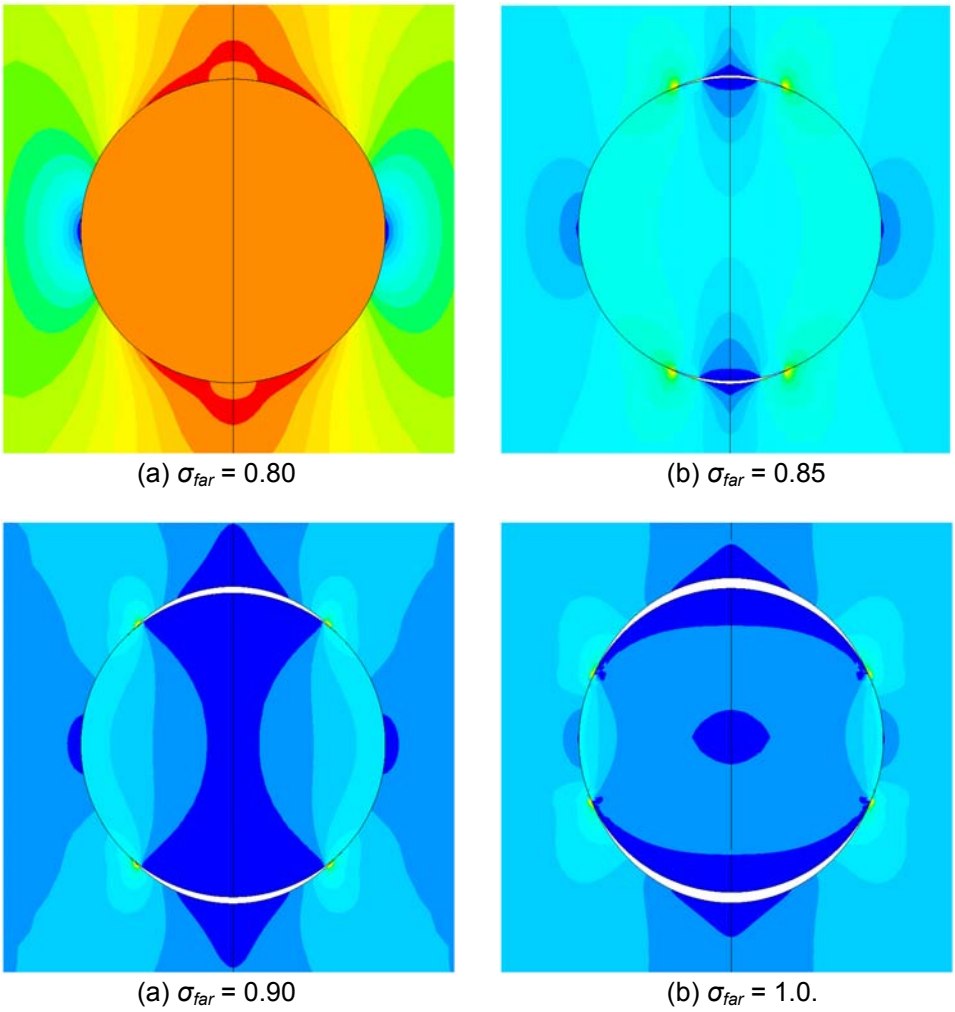

(a) σ_{far} = 0.80 (b) σ_{far} = 0.85

(a) σ_{far} = 0.90 (b) σ_{far} = 1.0.

Fig. 2. Single fiber two-side debonding

Remark. The model we consider clearly shows that, due to symmetry of geometry and loading, interface debonding develops at the opposite sides of fiber *simultaneously*. This simple (and quite predictable) fact raises the questions regarding the practical significance of numerous, from the early (Toya, 1974) to recent (Mantič, 2009) works where the similar LFM problems for a single fiber with constant interface toughness - but with one-side crack (in fact, improbable geometry!) - were considered. It will be shown below that two possible reasons of one-side crack formation are (a) variable interface toughness and (b) non-uniform stress field around the fiber.

To produce one-side interface crack in our model, we assume toughness of the bottom part of interface much higher as compared with the upper part. It suppresses development of the bottom crack: as seen from Fig. 3a, already for σ_{far} = 0.80 (before crack onset) the stress field becomes asymmetric in respect to *Ox* axis. It leads then to formation of crack at the upper side of fiber and partial (not complete) unloading of the bottom side, see Figs 3b - 3d.

In Figs 4 and 5, the interface normal and tangential stress distribution are shown obtained from the CZM (solid circles) and (for σ_{far} = 0.95, solid line) LFM models. It is clearly seen that LFM and cohesive zone model give practically identical results which can be regarded as the validation of both the developed analytical theory and presented here numerical data. The subtle difference is observed only in a close vicinity of the crack tip, where LFM assumes the stress to grow infinitely whereas CZM keeps them finite. Instead, in CZM we have a process zone of finite length where the interface is weakened - but not completely separated yet. However, their most

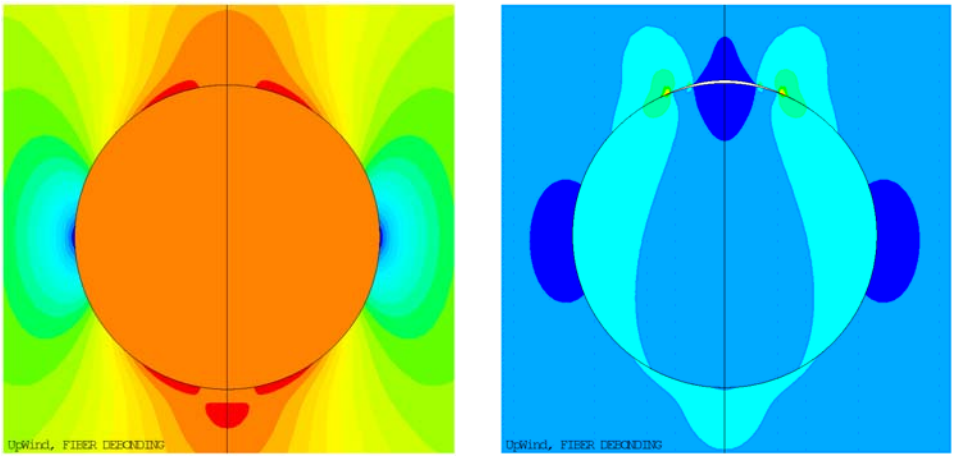

(a) σ_{far} = 0.80 (b) σ_{far} = 0.85

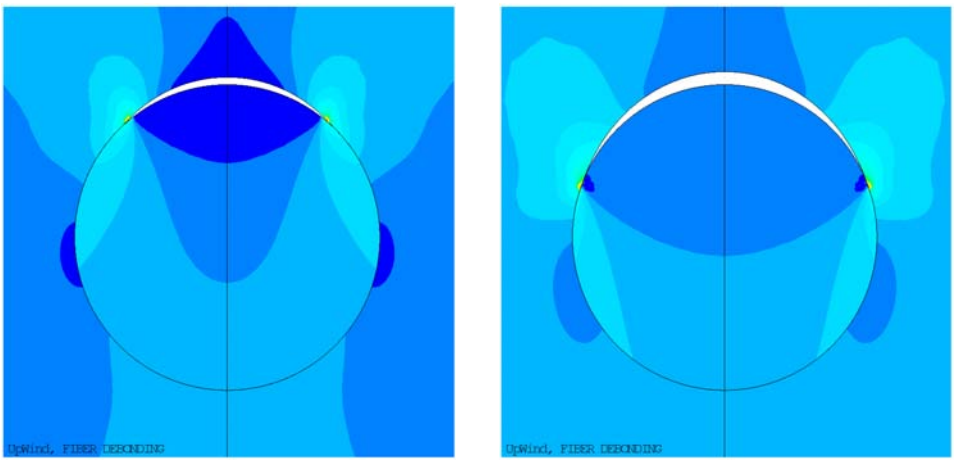

(a) σ_{far} = 0.90 (b) σ_{far} = 1.0.

Fig. 3. Single fiber one-side debonding

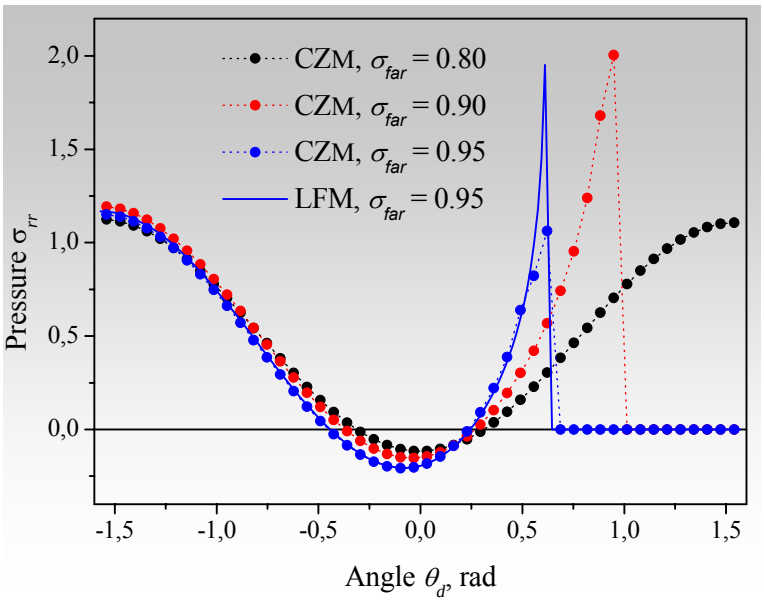

Fig. 4. Normal stress evolution during the interface crack formation

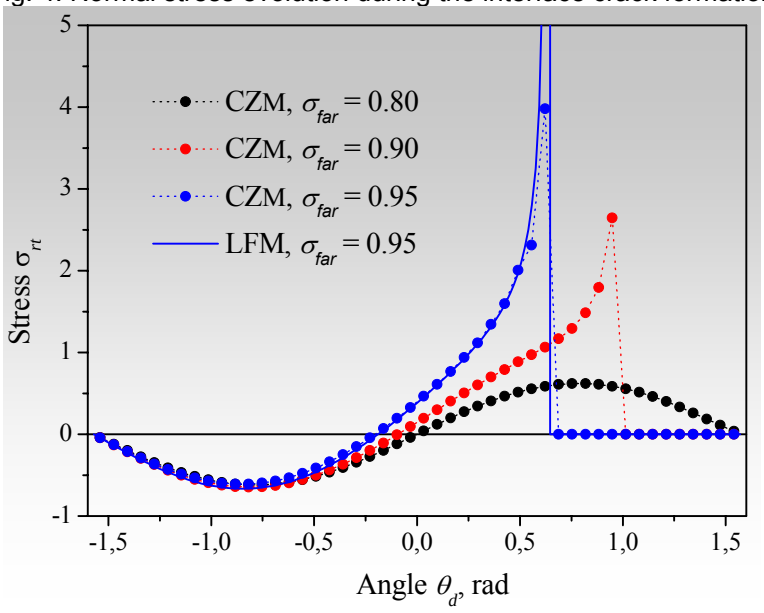

Fig. 5. Tangential stress evolution during the interface crack formation

principal difference consists in that the cohesive zone model describes crack nucleation and propagation whereas LFM cannot do it.

2.2. Comparison with experiment

The model we have suggested needs to be verified vs experimental data. Unfortunately, a very few publications can be found in literature where the interface toughness parameters were studied. In this and subsequent numerical study we adopt the numbers reported by Zhang et al. (1997) and Varna et al (1997) where the transverse tension tests were conducted for a single glass fiber embedded into the epoxy matrix. The reported there elastic moduli

- matrix material (Ciba Geigy LY 5052/HY 5052 epoxy resin): ν_m = 0.33, E_m =2.8 GPa;
- E-glass fiber (supplied by Owens Corning, 17 μm in diameter): ν_f = 0.22, E_f =71 GPa.

According to supplier, tensile strength of fully cured epoxy matrix is 80 - 86 MPa.

By matching the Toya (1974) model to the experimental observations Zhang et al. (1997) and Varna et al (1997) have estimated the interface toughness as G_c = 2 N/m in the case of absence the coupling agent (NOCA) and G_c = 10 N/m when the coupling agent was added (CA). The similar interface toughness values were reported recently by Caimmi and Pavan (2009). The matrix-fiber debonding was observed at tensile stress σ_{far} equal in average to 40 MPa (NOCA) and 75 MPa (CA). The interface strength σ_c was not estimated there: however, It follows from the above numerical study that it should be close σ_{far}.

For the assigned properties, the introduced above dimensionless criterion in both cases gives $G^* = E^* G_c/\sigma_c^2 R \approx 0.5$, i.e. the condition G_c << 1 does not meet. It means that the LFM model cannot be applied here and we can expect somewhat different behavior of interface. The two-side and one-side crack development scenarios shown in Fig 6 supports this thesis. Indeed, their comparison with similar data in Fig 3 says that, in contrast to LFM model, in the case G_c ~ 1 we have a jump-like *instantaneous* formation of finite size interface crack, with subsequent steady growth due to load increase. Determination of the minimum possible crack size defined by the interface strength to toughness ratio is the problem deserving a separate study.

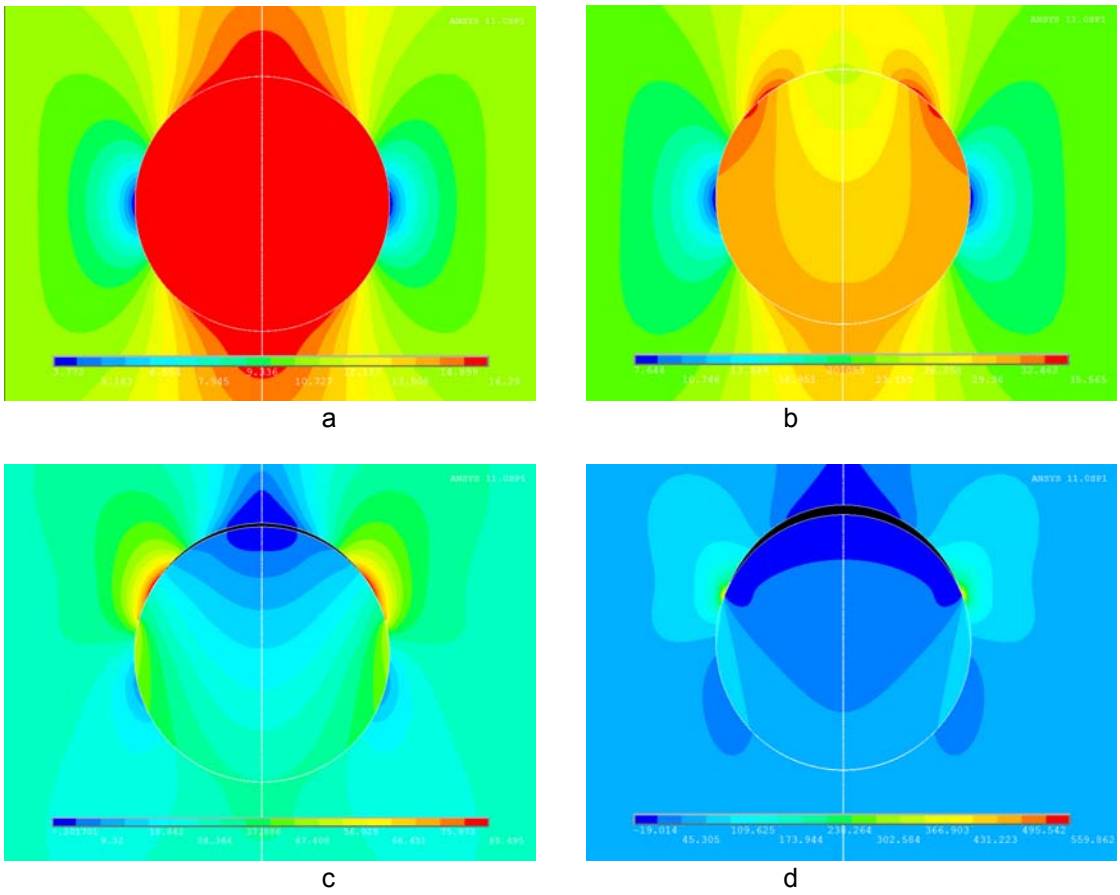

Fig. 6. Single fiber one-side debonding : G_c = 0.5

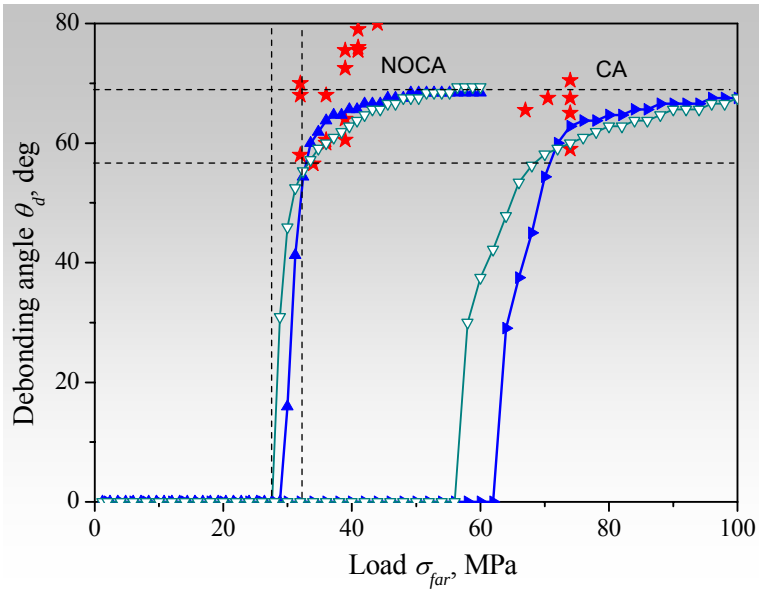

Fig. 7. Debonding semi-angle vs load: comparison with experiment

Some idea of quantitative predictive potential of our model can be drawn from Fig. 7, where the debonding semi-angle is shown as a function of applied far load. The stars represent the experimental data by Zhang et al. (1997), the line-connected triangles show the results of numerical analysis. There was an uncertainty in σ_c definition so calculations were performed for two distinct σ_c values. The open and solid triangles in Fig. 7 correspond to σ_c equal to 25 and 30 MPa, respectively, in the NOCA case and 50 and 60 MPa in the CA case. As seen from the plot, correlation between the model and experiment is quite satisfactory for the semi-angle values up to 70º. The model predicts this value to be limiting for a given composite: further loading leads, instead of crack propagation, to considerable stress concentration in the matrix and crack kinking. It seems plausible that large (of order 90º) debonding semi-angle observed by Zhang et al. (1997) are caused by the partial matrix destruction or other reasons not considered in our model. Noteworthy also that in the experiment an interface crack started from pre-existing crack and propagated along the fiber as well, i.e. the stress around the fiber may differ from the 2D plane strain considered by us.

3. Two-fiber model: debonding affected by interaction

We mentioned already that the interface crack nucleation is sensitive to the stress field around the fiber. The one-fiber problem considered by us in the previous subsection, is often (probably, too often!) used for evaluating the local stress in FRC. Needless to say, this model is has nothing to do with the real high-filled fibrous composite where the stress concentrations due to fiber-fiber elastic interaction play a dominant role. These concentrations will dictate, most

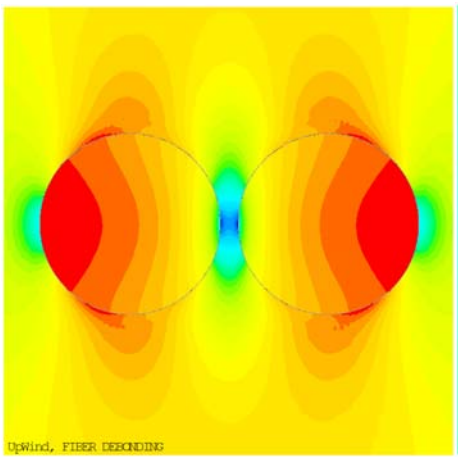

(a) σ_1 = 0.80

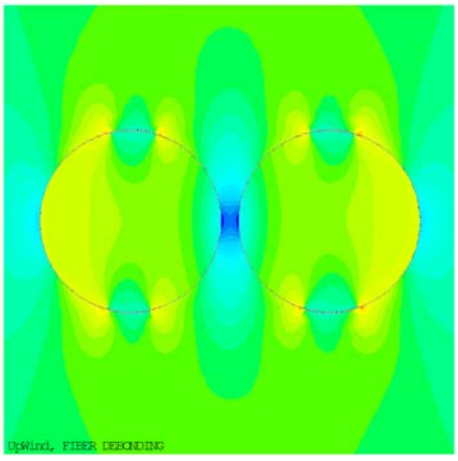

(b) σ_1 = 0.85

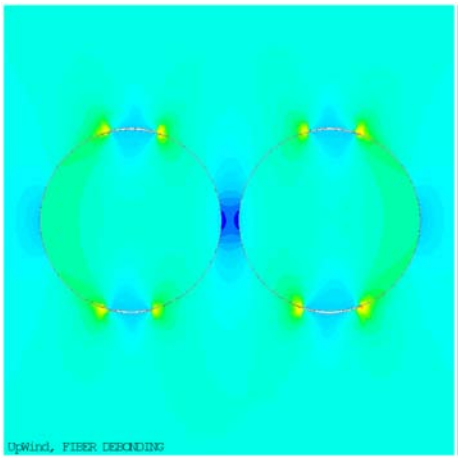

(c) σ_1 = 0.90

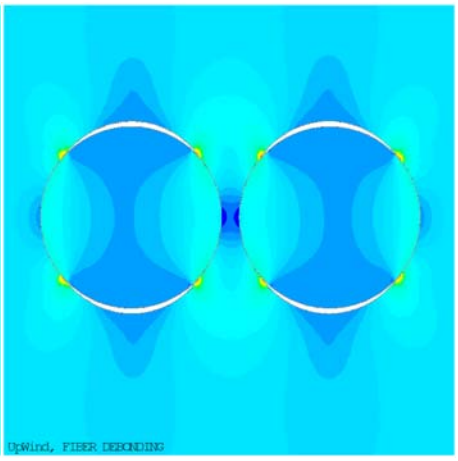

(d) σ_1 = 1.0

Fig. 8. Two-fiber model: $\theta_{12} = \pi / 2$

likely, also the place and moment of interface crack onset. We start studying this issue with two-fiber problem and consider various scenarios of crack growth depending on the mutual position (distance and angle). For simplicity sake, we perform simulations for the case of low ($G^* = 0.004$) interface toughness where LFM model is still valid. For larger G^* situation is simialr, with a few exceptions which will be discussed later on.

The presented at Figs 8 - 10 isolines of max principal stress σ_1 demonstrate an effect of the pair of fiber orientation angle θ_{12} with respect to the loading direction, namely, y-axis. We keep the distance between the centers of fibers R_{12} constant and equal 2.2 R. In the case $\theta_{12} = \pi / 2$ interactions between the fibers is moderate and interface debonding occurs in a way similar for that for a single fiber (see Fig. 8). As a result, we get two-side cracks on each of the fibers, Fig 8d. In the case $\theta_{12} = \pi / 4$, situation is quite different: here, the so-called shielding effect suppresses interface crack nucleation between the fibers and the outer one-cracks grow first. Only after they reached the limiting size, the opposite side of fiber starts to debond: note, that position of this crack deviates considerably from the inter-fiber zone where the matrix deformation and hence debonding is constrained by the much more stiff inclusions.

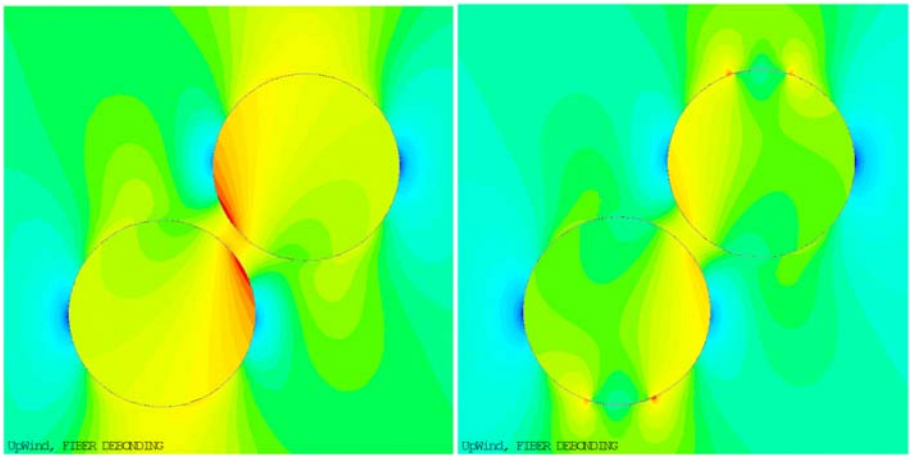

(a) $\sigma_1 = 0.70$ (b) $\sigma_1 = 0.80$

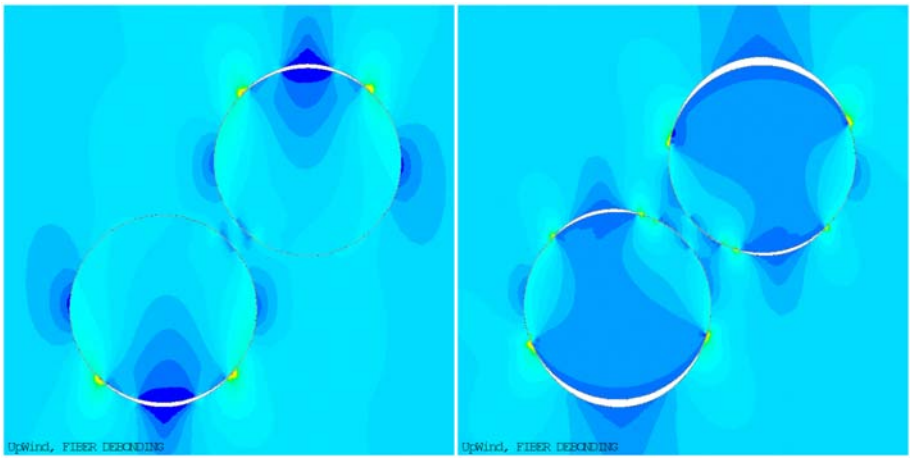

(c) $\sigma_1 = 0.90$ (d) $\sigma_1 = 1.0$

Fig. 9. Two-fiber model: $\theta_{12} = \pi / 4$

The case $\theta_{12} = 0$ is, however, the most favorable for the interface crack formation. In Fig. 10a one can see rather high localized stress concentration in the inter-fiber area. Already at $\sigma_1 = 0.40$ (Fig. 10b) we have two distinct stress concentration points which will became soon the

crack tips. At σ_1 = 0.60 (Fig. 3.12c) we have already the open crack and σ_1 = 0.80 (Fig. 10d) the cracks have reached the equilibrium state. In contrast to Fig. 9, here the one-side interface cracks have grown between the inclusions. The situation is somehat more involved for larger G^*: as was already mentioned, in this case we observe jump-like crack formation. It rather difficult to provide two simultaneous "jumps": a subtle variation of interface strength - or even finite accuracy of numerical method - may lead to situation where one crack develops first. This, in turn, leads to stress re-distribution and their relaxation in the inter-fiber area - and results in delay or supressing the another fiber debonding.

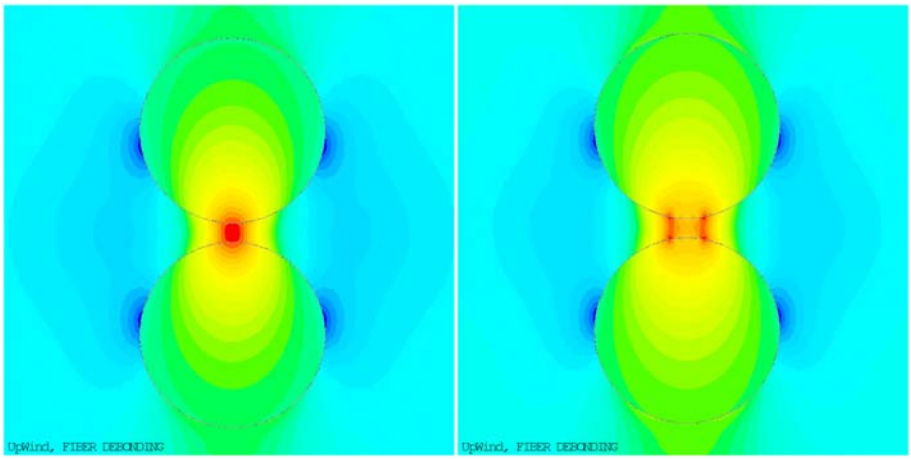

(a) σ_1 = 0.20 (b) σ_1 = 0.40

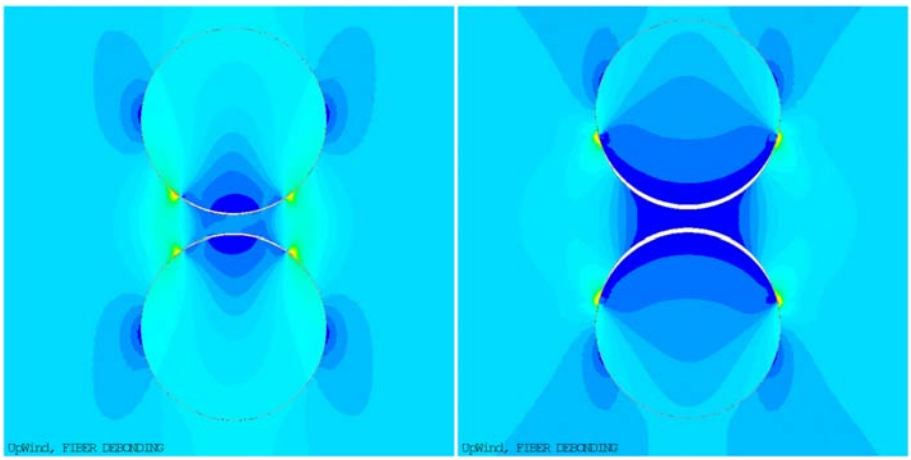

(c) σ_1 = 0.60 (d) σ_1 = 0.8

Fig. 10. Two-fiber model: θ_{12} = 0

The presented data show clearly that crack nucleation is indeed very sensitive to the stress fluctuations around the fiber and thus the many-fiber model is the *pre-requisite* for reliable prediction of progressive debonding in fibrous composite.

4. FCM and RUC models of progressive debonding: interface crack cluster formation and stiffness reduction

We consider two many-fiber models of fibrous composite, namely, the finite cluster model (FCM) and the representative unit cell (RUC) model. The first one is a matrix containing a finite array of fibers arranged in that or another way. RUC model represents an infinite periodic

structure, an elementary unit cell of which contains a certain number of inclusions: the whole volume of composite is obtained by replicating the cell in two orthogonal directions.

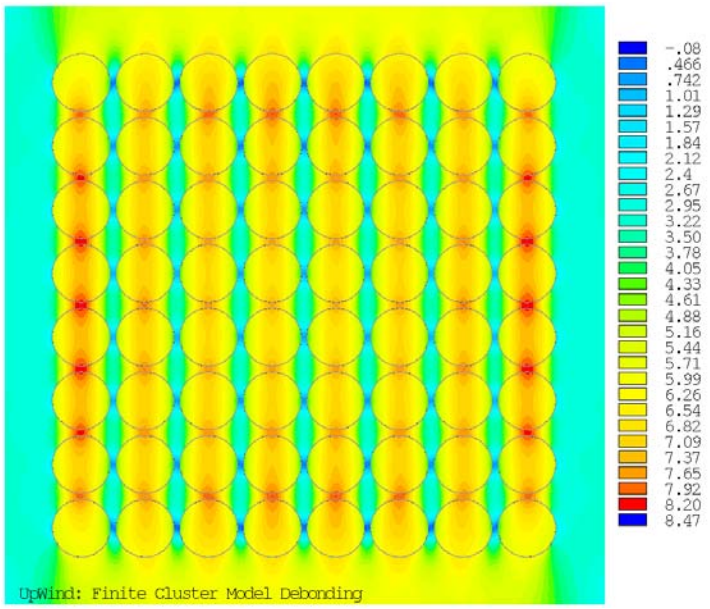

Fig 11a. Regular structure FCM: shielding effect

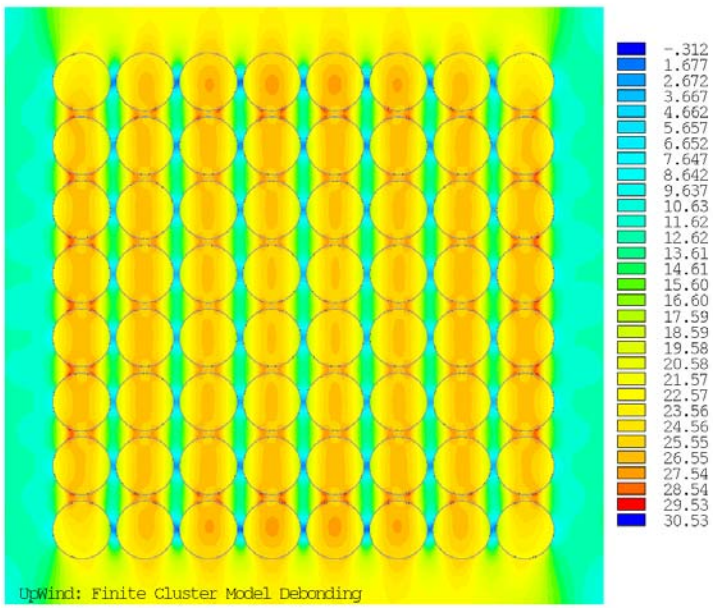

Fig 11b. Regular structure FCM: stress concentration in the points of potential crack tips

We start with the FCM model containing 64 fibers arranged in a square array. The properties used in simulation correspond to those reported by Zhang et al (1997), NOCA case. Figs 11a - 11d show stress field evolution and crack formation. At the early stage of loading (Fig 11a) the peak stresses locate between the fibers, then they divide and move to points of potential crack tips (Fig 11b). Next, two lines of interface cracks at the first and last fiber rows develop (Fig 11c). It lead to substantial stress re-distribution and at the final step, (Fig 11d) the

stress in the matrix between the cracks exceed the matrix tensile strength. It means that interface cracks will kink in the matrix and coalesce into macro crack.

This analysis correctly predicts the main steps in interface crack cluster formation. At the same time, it shows a drawback of FCM model consisting in that the outer fibers are more heavily loaded as compared with the inner ones (Fig. 11a). This effect manifests itself also in the more realistic FCM, with randomly placed fibers (Fig. 12). Here, we again get two crack clusters, nearby the top and bottom of the model, respectively, and one extra cluster in the central part of model. Noteworthy, all these clusters are oriented across the loading direction.

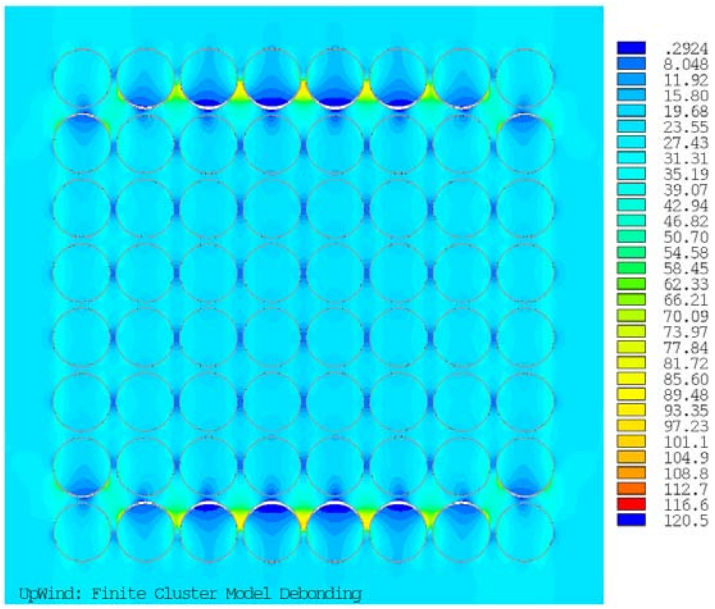

Fig 11c. Regular structure FCM: debonding onset

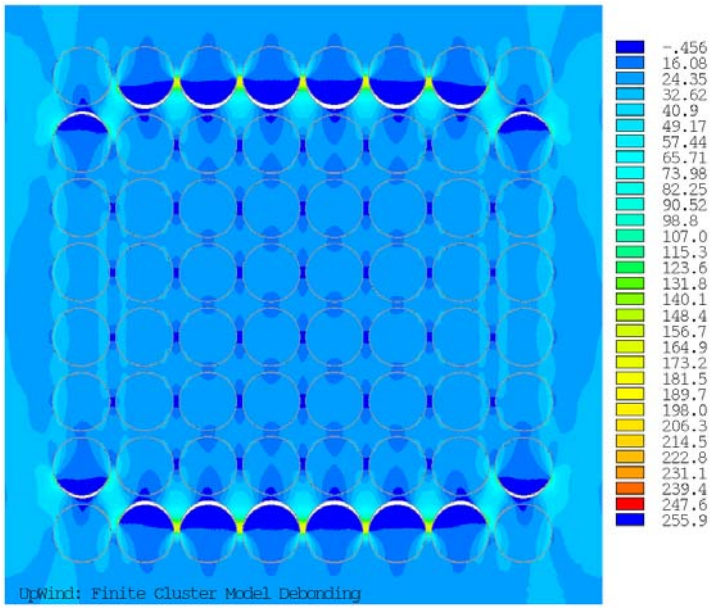

Fig 11d. Regular structure FCM: debonding growth and coalescence into macro crack

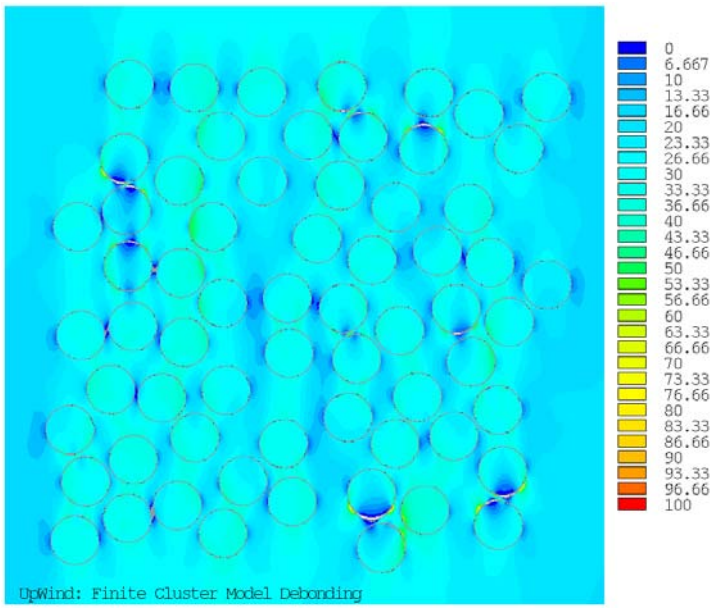

Fig 12a. Random structure FCM: debonding growth (σ_{far} = 28 MPa)

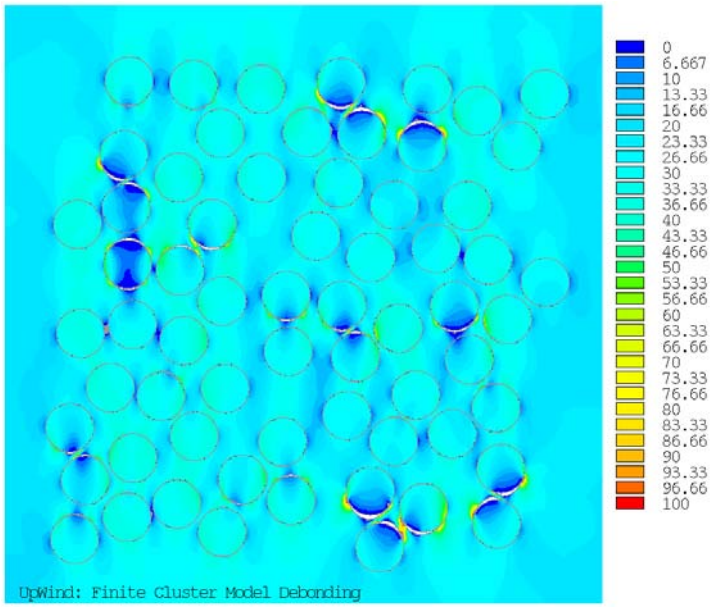

Fig 12b. Random structure FCM: debonding growth (σ_{far} = 32 MPa)

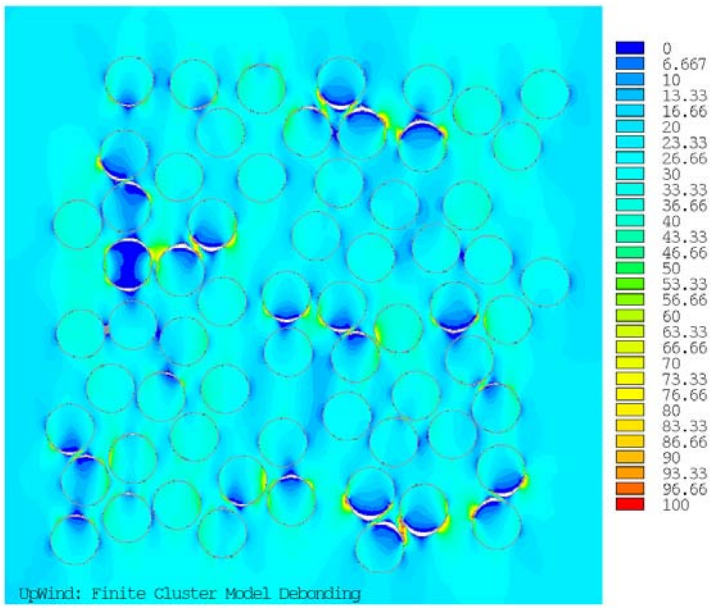

Fig 12c. Random structure FCM: debonding growth (σ_{far} = 36 MPa)

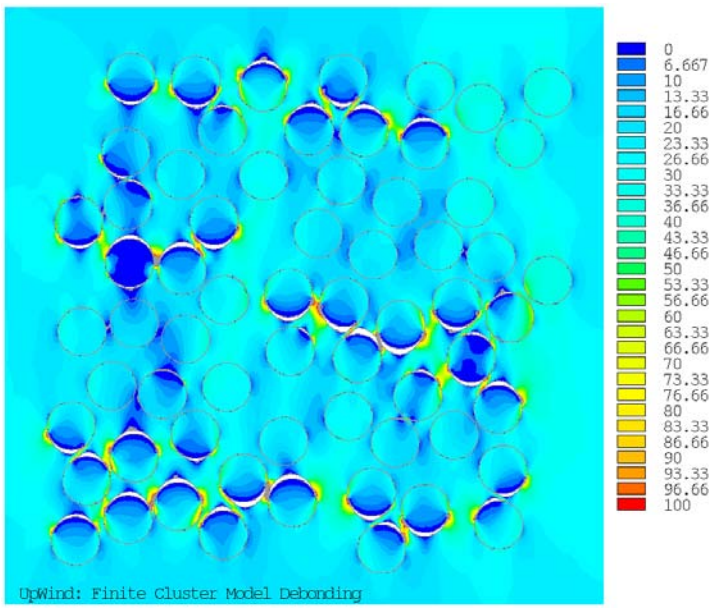

Fig 12d. Random structure FCM: debonding growth (σ_{far} = 40 MPa)

The principal and, probably, crucial advantage of RUC model consists in that it eliminates the discussed above edge effect completely and provides the most realistic description of local stress field in FRC. One can expect therefore this model to be also the best in simulation of progressive interface debonding phenomena. Typical debonding predicted by this model is shown in Fig. 14. It is clearly seen that it produces no edge effects and thus provides an

efficient simulation of progressive interface debonding and evaluation of the caused by debonding stiffness degradation and macroscopic anisotropy of fibrous composite.

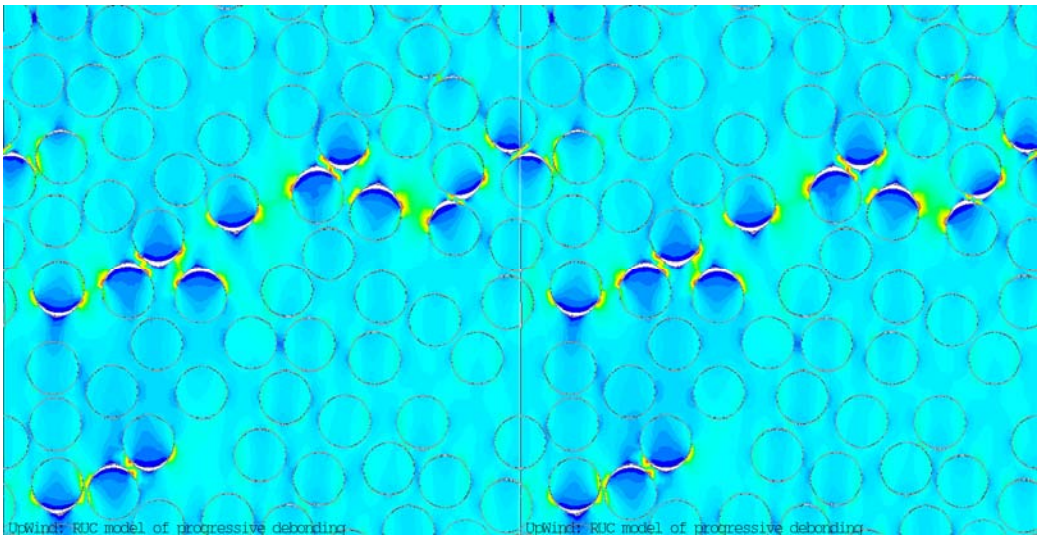

Fig 14. Random structure RUC: uniaxial loading in y-direction, 0.65% y-strain

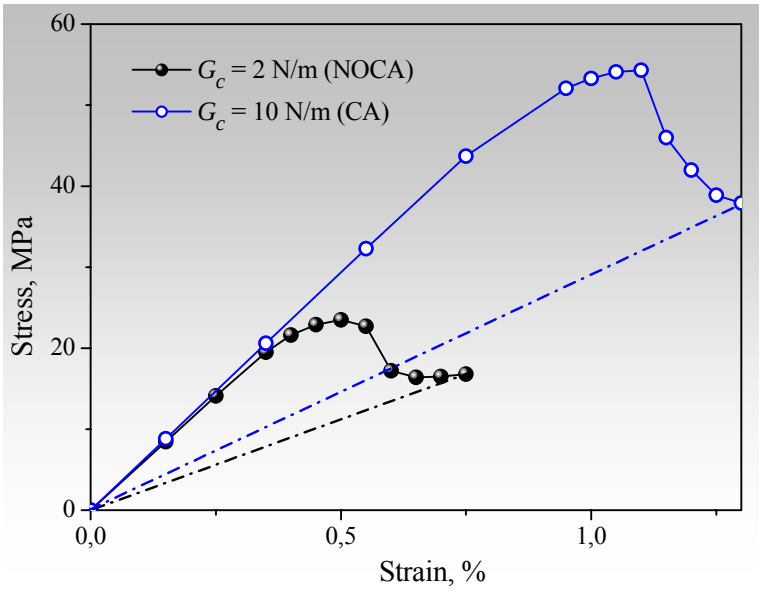

Fig. 15 Elastic stiffness reduction due to interface debonding

The FRC stress-strain curves obtained from this model is shown in Fig. 15. Noteworthy, matrix and fibers deform elastically so their non-linear behavior is entirely due to progressive interface damage. The irreversible strain does not accumulate: unloading is linearly-elastic, with reduced Young modulus (dash-dotted lines in Fig. 15). Effective stiffness, strain-induced anisotropy and even strength limit of FRC can be estimated using these data. On the other side, comparison of the predicted by model stress-strain curves with analogous experimental data would help to refine the parameters entering the CZM model of interface.

5. Conclusions

The interface stress grows up rapidly in the area between the fibers perfectly bonded with matrix. **In terms of strength**, it means that one can expect the interface crack onset at the far load well below the level predicted by the single-fiber model.

Partial interface debonding causes substantial stress re-distribution and relaxation of the peak interface stress on the neighboring fibers. **In terms of strength**, it means that the interface crack formation on a given fiber prevents debonding the nearest neighbor fibers. As to the stress relaxation degree, it depends on the crack size and the inter-fiber distance.

The stress intensity factors and the strain energy release rate are greatly contributed from elastic interaction between the fibers and are rather sensitive to the fiber arrangement. **In terms of strength**, it means that the interface crack propagation/stopping is mediated by the neighbor fibers and cracks.

The adequate model of the progressive interface debonding in FRC must take all these factors into account. It is clear that the single fiber model fails completely and the only way out is to deal with the multiple fiber models. Among them, the representative unit cell model is, probably, the best choice.

References

1. Alfano, G., Crisfield, M.A., 2001. Finite Element Interface Models for the Delamination Anaylsis of Laminated Composites: Mechanical and Computational Issues. International Journal for Numerical Methods in Engineering 50, 1701-1736
2. Barenblatt, G.I., 1962. The mathematical theory of equillibrium cracks in brittle fracture. Advances in Applied Mechanics 7, 55–129.
3. Caimmi F, Pavan A. An experimental evaluation of glass–polymer interfacial toughness. Engng Fract Mech (2009), doi:10.1016/j.engfracmech.2009.06.014
4. Cornett P., Pugno N., Carpinteri A. et al., 2006. Finite fracture mechanics: A coupled stress and energy failure criterion Engineering Fracture Mechanics 73, 2021–2033
5. Dugdale, D.S., 1960. Yielding of steel sheets containing slits. Journal of the Mechanics and Physics of Solids 8, 100–104.
6. Kushch, V.I., 2010. Transverse conductivity of unidirectional fibrous composite with interface arc cracks. International Journal of Engineering Science 48, 343–356
7. Kushch, V.I., Shmegera, S.V., Mishnaevsky L., 2008. Meso cell model of fiber reinforced composite: interface stress statistics and debonding paths. International Journal of Solids and Structures 45, 2758-2784.
8. Kushch, V.I., Shmegera, S.V., Mishnaevsky L., 2009. Elastic interaction of partially debonded circular inclusions. I. Theoretical solution, submitted to International Journal of Solids and Structures
9. Kushch, V.I., Shmegera, S.V., Mishnaevsky L., 2009. Elastic interaction of partially debonded circular inclusions. II. Application to fibrous composite, submitted to International Journal of Solids and Structures
10. Leguillon, D.. 2002. Strength or toughness? A criterion for crack onset at a notch European Journal of Mechanics A/Solids 21, 61–72

11. Leguillon D., Piat R., 2008. Fracture of porous materials – Influence of the pore size. Engineering Fracture Mechanics 75, 1840–1853

12. Li, S., Thouless, M.D., Waas, A.M., Schroeder, J.A., Zavattieri, P.D., 2005. Use of mode-I cohesive-zone models to describe the fracture of an adhesively-bonded polymer-matrix composite. Composites Science and Technology 65, 281–293

13. Mantič, V., 2009. Interface crack onset at a circular cylindrical inclusion under a remote transverse tension. Application of a coupled stress and energy criterion. International Journal of Solids and Structures 46, 1287-1304.

14. Needleman, A.A, 1987. continuum model for void nucleation by inclusion debonding. J Appl Mech 54, 525–531

15. Taylor, D., 2008. The theory of critical distances. Engineering Fracture Mechanics 75 (2008) 1696–1705

16. Toya, M., 1974. A crack along interface of a circular inclusion embedded in an infinite solid. Journal of the Mechanics and Physics of Solids 22, 325-348.

17. Tvergaard, V., Hutchinson. J.W., 1992. The relation between crack growth resistance and fracture parameters in elastic-plastic solids. J Mech Phys Solids 40,1377–1397

18. Ungsuwarungsri, T., Knauss, W.G., 1987. Role of damage-softened material behavior in the fracture of composites and adhesives. Int J Fracture 35, 221–241

19. Varna, J., Berglund, L.A., Ericson, M.L., 1997. Transverse single-fibre test for interfacial debonding in composites: 2. Modelling Composites Part A 28A, 317-326

20. Xu, X-P, Needleman, A., 1994. Numerical simulations of fast crack growth in brittle solids, Journal of the Mechanics and Physics of Solids 42, 1397-1434

21. Zhang, H., Ericson, M.L., Varna, J., Berglund, L.A., 1997. Transverse single-fibre test for interfacial debonding in composites: 1. Experimental observationsComposites Part A 28A, 309-315